

AO13 Aerosol sampling

supervisor: Dr Daniel Peters

March 2008

Abstract

The vertical distribution of aerosol properties in the atmosphere, for example- salt crystals, sand, ablated soils, and aviation derived black carbon soot in the upper troposphere and lower stratosphere is very poorly quantified. Yet they have a significant impact on radiative transfer in an aerosol laden atmosphere. There has been relatively little research involving direct sampling of aerosol particles at altitude, and published studies have involved aircraft mounted samplers.

A cheap autonomous sonde mounted sampler was designed and constructed together with functional sonde sub-systems, to enable sampling to be conducted over the UK at altitudes up to 30km, with multiple samples taken in different altitude ranges. The sampling device was designed to enable examination with a scanning electron microscope to determine composition, morphology, and particle concentrations to be inferred.

1 Introduction

Aerosol research is a very active field, with particular bearing on many aspects of atmospheric physics. However, the majority of non ground based studies have involved inferring measurements from satellite, not direct measurements or sampling. Blake and Kato [1], and Pusechel et al [3], employed NASA ER-2 and DC-8 research aircraft mounted sampling devices. These aircraft have altitude ceilings of 21Km and 12km respectively, lower than sonde flights, which

can reach 30km with ease. In Europe there is also the CARIBIC program [4], employing an Airbus A340 and Boeing 767 300ER in published research programs. Physical sampling for later laboratory analysis allows chemical composition to be determined, along with particle nonsphericity or morphology [1].

Meanwhile, the falling price of electronic hardware including GPS receivers and communication equipment has sparked interest in the development of low-cost sounding units to supplement the traditional radiosonde network. A sonde based system is considerably cheaper and more flexible than the aforementioned systems, can sample a greater altitude range, and is not limited by air traffic control regulations to the same extent. This project was inspired by such novel alternative sounding methods, which have recently been pioneered in the UK by the UK high altitude society [10], and Cambridge university spaceflight [11].

2 Methods

2.1 Science Aims

With any such project involving a large design element a clear set of science aims as initial targets is essential for efficient planning. A set of aims were drawn up as follows;

1. Stratospheric sampling:
2. Tropospheric sampling:

From a consideration of the science aims, the list of requirements were drawn up;

2.1.1 Science Requirements

1. The collection efficiency as a function of particle size should be well quantified
2. The sampler should collect a statistically significant sample
3. There should be statistically insignificant sample contamination
4. Non-volatile particles should be captured and stored without changes to their chemistry
5. If multiple samples are taken (e.g. differing altitude ranges) then cross contamination should be insignificant or at least well quantified

2.2 Hardware design considerations

A typical sonde flight will ascend to reach an apogee altitude of 20 to 30Km above mean sea level around 2 hours after launch. The latex envelope then bursts, leaving the payload to descend by parachute.

Ground air temperature in the UK is usually in the 10 to 20°C range, and tropopause temperatures are typically around -50°C, so the payload experienced large temperature changes. The lower temperature limit lies outside the standard industrial

temperature range used for electronics, which extends to -40°C. During descent into the troposphere, condensation is a significant risk due to the sonde payload being below the dew-point. The typical solution to these difficulties, adopted by members of UKHAS

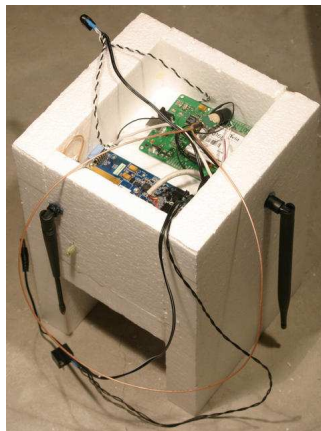


Figure 1: A typical sonde based on an embedded linux system

and others is a 25 to 50mm thick airtight¹ enclosure fabricated from extruded polystyrene or expanded polypropylene. This serves to protect sensitive components on landing, as well as allowing the electronics to increase the internal temperature to acceptable levels.

The avionics are critical to safely recovering the payload after landing, and again UKHAS[10] and CUSF[11] provide useful examples of how to design a successful system. Typically a central computer board based around a micro-controller, or an off the shelf single board Linux machine is used. The other electronic hardware is then interfaced with the central “motherboard”, a minimal architecture consisting of GPS receiver, mobile phone/GSM module module, radio module, and a release mechanism to cut-down² Such a system typically requires in the order of 1 to 2 Watts of electrical power, and it has been found that lithium camera batteries, such as sold by energizer[12] offer the best performance, the data-sheet listing the absolute minimum operating temperature as -40°C.

The radio module is perhaps one of the more difficult components, in the UK OFCOM limits transmissions from high altitude balloons to 10mw on the 434MHz band, using a commercial transmitter module of a licenced design. It is possible to transmit radio-teletype at 300 baud on this band for several hundred kilometres by using a pulse shaping transmission scheme to modulate an FM transmitter. Members of the UK high altitude society have previously designed a system, but the source code has not been released, and there is no printed circuit board design for the project. With this in mind, in 2007 the author designed a radio module using an 8 bit AVR micro-controller, which was employed for the first time on this sonde.

A final consideration is mass, the civil avia-

¹obviously an airtight closed cell foam enclosure would suffer structural failure due to internal overpressure during ascent, but assembly has been found to never be good enough to be completely airtight, although sufficient to prevent condensation

²“cut-down” is a radiosonde term meaning to trigger an early descent by releasing the balloon from the payload, for example to avoid landing in water

tion authority does not explicitly set mass limits on radiosondes, but bearing in mind health and safety, and insurance for the project, a mass limit of 2Kg was decided upon.

2.3 Instrument design process

The instrument designs considered were all drawn from Hinds [2], and evaluated on their suitability based on the science aims and hardware considerations, along with our budgetary limits of approximately £1000 for the entire system. From Blake and Kato[1], number densities of stratospheric particles are in the $10^4 m^{-3}$ to $10^5 m^{-3}$ range, so a cubic meter of air might be required to provide statistically significant data for particle morphology and chemistry studies, if our instrument has a collection efficiency in the 10% range and a sample of 10^3 particles is required. If multiple samples are to be taken during the ascent, a reasonable sampling time might be around 40 minutes, or 2×10^3 seconds. This gives a flow rate of between 10^{-1} and 10^{-2} litres per second through the instrument.

In all the sampling techniques considered, particles are deposited onto some sampling surface for later analysis. For analysis of with a scanning electron microscope, a minimum number density on the sampling surface of 1 particle per $100 \mu m^2$ seems reasonable³. For a sample of 10^2 to 10^3 particles, this corresponds to a sampling surface area $0.33 mm^2$ at most. Assuming that the airflow cross-section is larger than the sampling surface area (valid in all approaches except 4), then with a cross section of $1 mm^2$ for our airstream through the instrument, an airspeed of at least $10 ms^{-1}$ is required. The Reynolds number is given by

$$\frac{\rho v_s L}{\mu} = \frac{v_s L}{\nu} \quad (1)$$

For typical stratospheric flow, $\mu = 2.5 \times 10^{-5}$, and $\rho = 10^{-1} Kg/m^3$, so the Reynolds number is

³simply by considering the difficulties inherent in using a scanning electron microscope to examine a sparsely populated sampling surface

given by

$$\frac{10^{-1} v_s L}{2.5 \times 10^{-5}} = 4 \times 10^3 v_s L \quad (2)$$

Within circular pipes the critical Reynolds number is generally accepted to be 2300, where the Reynolds number is based on the pipe diameter and the mean velocity V_s within the pipe. Assuming the lower bound on volumetric sampling rate, i.e. 10^{-2} Litre s^{-1} then if our instrument consists of some circular pipe.

$$\pi L^2 V_s = 10^{-5} \quad (3)$$

so, if $Re < 2000$ then

$$V_s L < 0.5 \longrightarrow L \gtrsim 10^{-4} \quad (4)$$

in the lower troposphere, the Reynolds number will be an order of magnitude higher, so the condition on L will increase by an order of magnitude, but 1mm diameter is achievable, and lower flow rates will be required due to the higher volumetric number densities of particulates in the troposphere. So, in conclusion, achieving laminar flow is possible, but achieving a well characterised sampling efficiency, and a high particle density on the sampling surface is non trivial. Laminar flow is especially important for the first three methods, as existing studies have been in the laminar flow region, and collection efficiencies in the case of electrostatic and thermal precipitators especially, drop off precipitously as we enter the turbulent flow regime. Four approaches were considered:

1. Thermal precipitator: as this system relies on a temperature gradient, it would require a heater, probably a resistance wire. Power limitations make this hard to achieve. As with a filter, achieving a high particle density per unit area of the deposition surface is difficult. A small heated area separated from the deposition target by an air gap would require a high airflow velocity between the two plates, limiting the collection efficiency. If the airflow becomes non laminar, collection efficiency will drop off greatly, and an accurate efficiency calculation would require careful calibration.

2. Impactor: This design has been used with success before by NASA on ER-2 and DC8 aircraft [5], however an aircraft mounted implementation can easily have a very high velocity airstream, and high volumetric flow rate, something that is harder to achieve on a sonde with power, weight and size limitations. A small scale impactor may work well for small ranges of particle size, but designing for a large range of particle sizes from the hundreds of nanometre diameter to several micron range is hard, due to the widely differing Reynolds numbers that the particles would experience. Despite research into existing designs, an existing design that was well studied and easily adapted for sonde use was not found.
3. Electrostatic precipitator: the operating principle uses a corona discharge to charge particles, and then an electric field to draw them out of the airflow onto a collection target. The most common design is so called single stage, employing a sharpened electrode opposite a deposition target, hence achieving both ionisation from the corona discharge, and deposition from the E field in a single step. Yung-Sung Cheng et al [6], Laskin and Cowin [7] and Aerosol technology[2] all describe similar designs, which are well suited to sonde use. Yung et al also found efficiency curves for their single stage precipitator, based on Morrow et al [8]. This technique has the advantage that a standard scanning electron microscope or SEM sample holder can be used as a target plane, simplifying the particle analysis considerably.
4. Filter: This would appear a natural choice, but with the low particle densities in the stratosphere, a high flow rate per area of filter is required. However, in the limiting case where our pump generates a vacuum, the pressure across the filter is limited to atmospheric pressure. At the low atmospheric pressure at such altitudes, it is thus impossible to reach the required differential pressure

to achieve a usable particle density per unit area of filter with a pump downstream of the filter (flow through a filter is linear with differential pressure 6). A pump mounted upstream would lead to contamination and particle size bias problems. Also, the retrieval process would be extremely difficult with a fibre based filter- membrane filters would be similar to the other three techniques with regard to retrieval, but at the expense of lower flow rate than fibre based filter.

The electrostatic precipitator was chosen as the sampling system, primarily due to the existing and well researched designs, and suitability for use in a small, lightweight and low power instrument.

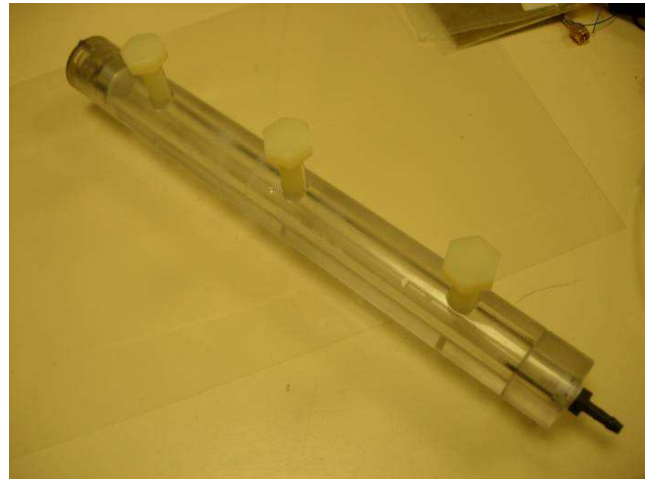


Figure 2: The electrostatic precipitator was machined from perspex, with a piston at the inlet to prevent contamination

Although this was a untried innovation, the relatively high collection efficiency found by Yung et al suggests that an inline sampling system with multiple target/ioniser pin pairs would be effective. A three sample device was designed, based on three variants of the design from Morrow et al. mounted in series in a solid perspex tube.

Unfortunately this design cannot reach the 0.33mm^2 deposition area target calculated earlier, instead the deposition takes place over an

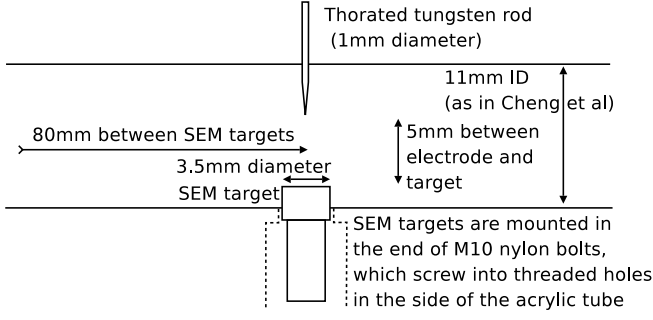


Figure 3: The design was based on Cheng et al, figure 1

area of around 6mm^2 , around 20 times lower particle density. However, with good handling to avoid contamination, it should be possible to locate the particles with some microscope panning.

2.4 Avionics

For maximum flexibility the avionics system was designed around the atmel ngw100 embedded linux board. This enabled flight software to be easily tested on a PC running the ubuntu distro. Serial ports were then used to interface with a daughter-board, phone, radio module, and gps module. The cut-down directly connected to GPIO for improved reliability. The ngw100 pulses GPIO high then low on bootup, so a binary coded decimal decoder IC was used to drive the cut-down MOSFETs.

The daughter-board was designed around an atmel atmega168 8 bit micro-controller⁴, mainly serving as an IO expander and ADC, but with the pulse width modulation output used to drive the pump on the sampling instrument. This arrangement allows for real time pump control based on an ADC reading from a differential pressure sensor connected across the filter between the precipitator tube and pump.

Air viscosity is a function of temperature, as described by Sutherland's equation

$$\eta = \eta_0 \frac{T_0 + C}{T + C} \left(\frac{T}{T_0} \right)^{3/2} \quad (5)$$

where C is Sutherland's constant (120K for air), T_0 is the reference temperature in kelvin

⁴also referred to as a μC

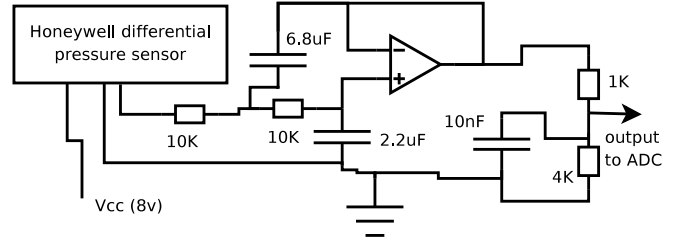


Figure 4: Circuit diagram of the Sallen-Key filter used for the differential pressure sensor

(291.15K for air), and η_0 is the reference viscosity (1.827×10^{-5} for air).

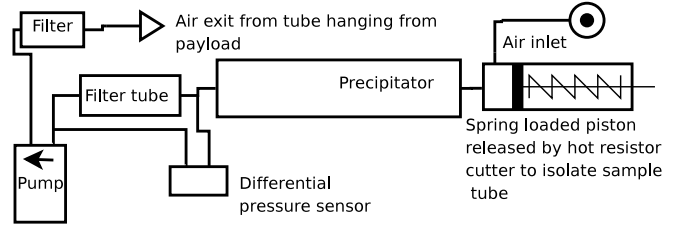


Figure 5: Flow diagram of the air sampling system

Over the typical temperature range that the sonde might experience, this leads to a significant change in viscosity, such that using predicted temperatures for the current altitude wouldn't not give a sufficiently accurate result. Hence a semiconductor band-gap based sensor IC (LM94022) was placed inside the exit tube from the precipitator directly in the airflow. Unfortunately this was damaged by a mistake during testing, and was replaced by a thermistor and preamp circuit.

The precipitator itself requires a high voltage supply for operation. Research into commercial systems lead to the design of a simple low cost supply employing a cold cathode inverter, designed for LCD back-lights, and giving an output of approximately 700v ac, followed by a cockroft Walton multiplier chain to boost the voltage. Switching voltages in the Kv range using transistors is quite difficult, so three separate supplies were constructed, one for each sampling electrode. Due to the lower dielectric strength of air at low pressures, the two upper atmospheric supplies only had one multiplier stage, giving

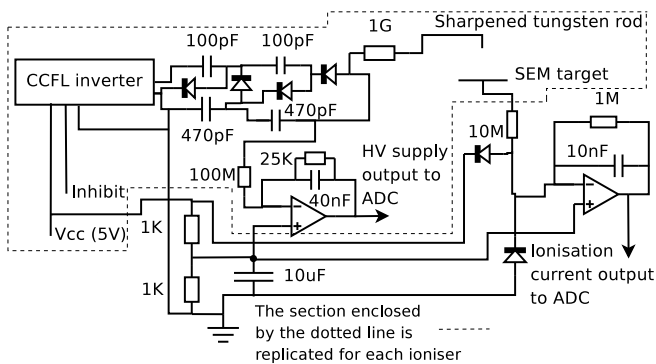


Figure 6: Circuit diagram of the electrostatic precipitator electronics

approximately 2.5Kv output, whereas the first stage supply had an output of approximately 5Kv. As suggested by Laskin and Cowin, 1G Ω resistors were placed between the HV supplies and the precipitator to stabilise the ionisation current. This had the additional advantage of ensuring high voltage safety, as the current is limited to a low level.

2.5 Software

There were two main pieces of software to be written, the main control code for the ngw100, in python, and the low level interface code for the μ C, in c, and compiled with avr-gcc.

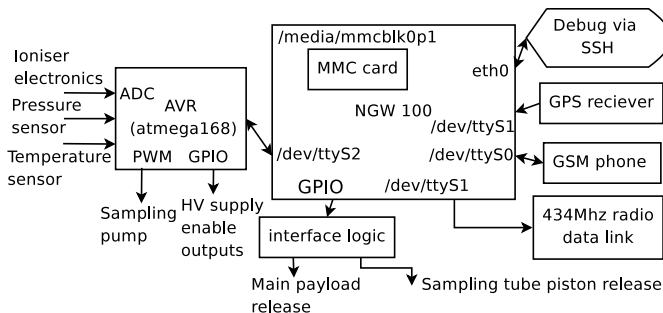


Figure 7: An overview of the payload as it appears from the software's perspective

The default kernel on the ngw100 does not allow access to the three available serial ports, so a kernel recompile was needed. The pyserial module was then used to interface with the the ports. There is little free space on the ngw100 flash memory, so an 128MB MMC card was used

to store data logs and mount python. As the 434MHz radio has a relatively high bit error rate, a reed-Solomon python module, written previously by the Author, was used to add forward error correction to the end of the data-packets, but leave the actual data human readable, to simplify ground station operation. The landing spot prediction code posted on the UK high altitude society website⁵ was ported to python, and the parachute drag constants rescaled to the 1.4 meter chute used for payload recovery. This was then combined with a polygon of the East Anglia coastline, and an "exclusion zone" north of London and east of Birmingham, to trigger the cut-down and avoid an urban or sea landing if necessary, and more basic routines for logging data and relaying telemetry. Communication with the phone was via the extended Hayes AT command set, and the gps via the standard NMEA serial protocol.

The μ C code made heavy use of procyon avrlib [9], a library simplifying tasks such as buffered serial IO and pulse width modulation.

Both programs are in the appendix, together with the radio modem source and the reed-Solomon module.

2.6 Testing

2.6.1 Aerosol flow testing

This used an ultrasonic nebuliser to generate a H₂O NaCl aerosol, followed by a diffusion dryer, then a hose that could be used to supply either the sonde payload, or a dilution unit, followed by an optical aerosol spectrometer. The diffusion dryer dehydrated the wet aerosol to give dry NaCl crystals. Aerosol output of this apparatus was observed to be relatively unstable upon being turned on, so the following graph (Figure 9) was obtained from an hour long test for calibration purposes.

The control loop on the AVR driven daughterboard was evaluated during the flow test. As expected the volumetric flow rate was found to be linear with differential pressure across the filter, as shown by Darcy's law, describing volumetric

⁵http://wiki.ukhas.org.uk/ideas:landing_spot_prediction

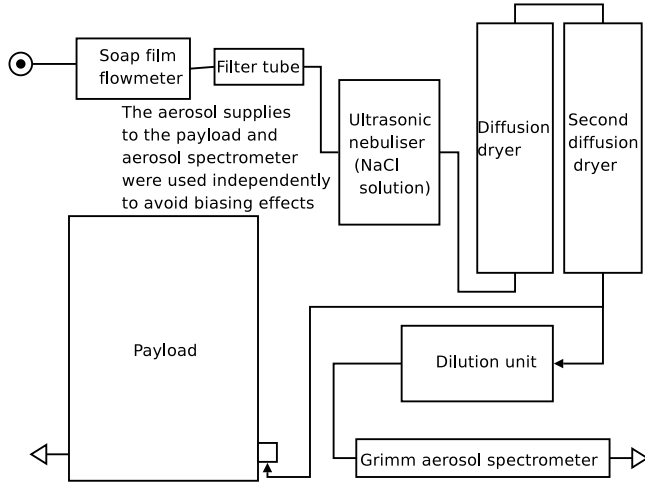


Figure 8: Schematic of the aerosol flow test experiment

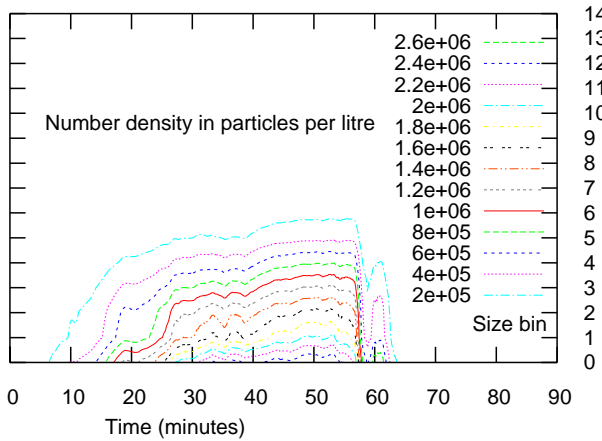


Figure 9: Contour plot of volumetric particle density from ultrasonic nebuliser against size bin, and run time

flow rate Q through a material of permeability κ .

$$Q = \frac{-\kappa A (P_b - P_a)}{\mu L} \quad (6)$$

In the case of a filter, L is the membrane thickness, and $P_b - P_a$ the pressure drop across the filter. μ is the dynamic viscosity of the airflow, itself a function of temperature, as described in equation 5.

However, a long term drift in flow rate was observed. In figure 10 the flow rate is shown together with an exponential fit, along with vol-

umetric flow rates at different feedback loop setpoints.

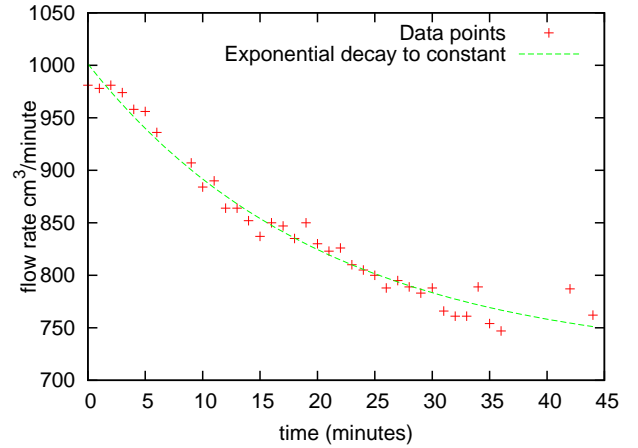


Figure 10: Test data over a 45 minute period, with an fit of the form $a \times e^{bt}$ where t is time in minutes

Variable	Final Value	Standard Error
a	= 282.896	+/- 12.64
b	= -0.0490468	+/- 0.00573
c	= 718.466	+/- 14.57

Table 1: Computed fit for figure 10

Setting different control loop setpoints for the μC , and fitting with a straight line of the form $y = ax + b$, figure 11 was obtained.

Tables 2 and 3 give the linear fit parameter. It is interesting to note that the gain of the system, or a in the tables, changes by only slightly more than one standard error ($\sqrt{3.437^2 + 1.29^2} = 3.6711$ as opposed to $43.14 - 38.7302 = 4.4098$, so it would appear that the exponentially falling response is due to the null of the pressure sensor, or b in our linear fit.

Variable	Fit Value	Standard error
a	= 43.14	+/- 3.437
b	= -87.3	+/- 79.69

Table 2: Linear fit to control system response at start of experiment

The change in the system null is $87.3 - 257.834 + \sqrt{40.19^2 + 79.69^2} = -170.53 + \sqrt{89.251}$. The predicted decay is given by

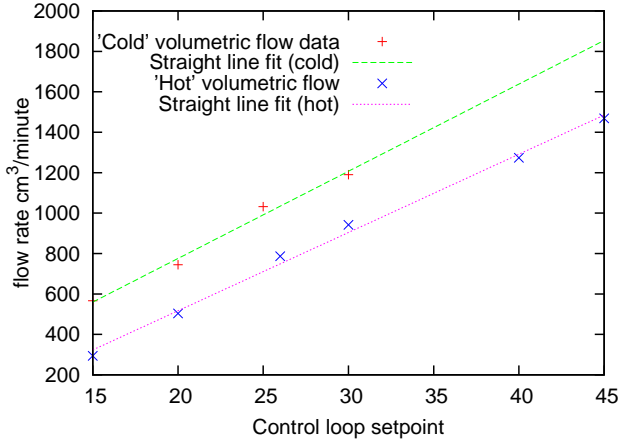


Figure 11: Data and linea fits for the control loop response straight after turn on, and after 45 minutes of operation

Variable	Fit Value	Standard error
a	= 38.7302	+/- 1.29
b	= -257.834	+/- 40.19

Table 3: Linear to control system response after 45 minutes

$282.896(e^{-45 \times 0.0490468} - 1) = -251.77$ so this is within standard errors. Hence in summary it appears that the pressure sensor null is responsible for the drift in volumetric flow rate. A simple change to the AVR firmware, to turn off the pump and recalibrate the differential pressure sensor every 15 minutes or therabouts was made to resolve the issue.

The electrostatic precipitator the main subject of the flow test evaluation. The nebuliser was planned to be on for 15 minutes, but it was found that the ioniser current dropped to zero after only seven minutes. This resulted in a collected aerosol weight only slightly greater than the accuracy of our balance. From the graph it would appear that a function of the form $a + be^{cx}$ fits the data reasonably. It seems reasonable to assume that this effect is due to the coating of salt deposited on the SEM target. As this is insulating, and negatively charged from the corona discharge, once an insulating layer has built up, a surface charge may accumulate, reducing the electric field between the electrode rod and target until corona discharge no longer occurs, and

the ionisation current drops to zero. In figure 11 the first, third and forth datapoints are not used in the fit, as the small increase in current at 2 minutes is believed to be due to increasing humidity as the nebuliser is turned on, not the target plane coating effect responsible for the current drop.

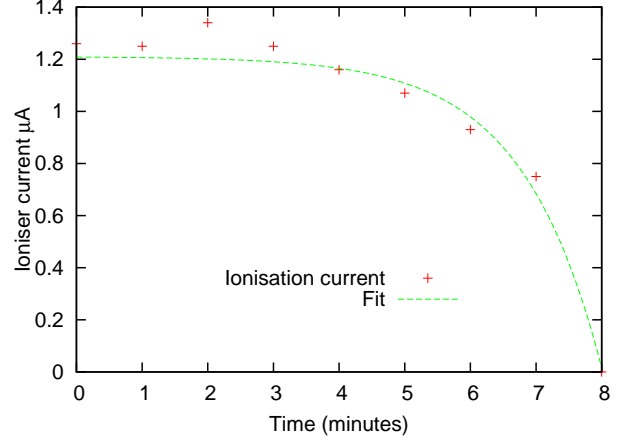


Figure 12: ioniser current plotted against time, with a function of the form $a + be^{cx}$ fitted to the data

Variable	Fit Value	Standard error
a	= 1.2101	+/- 0.04675
b	= -0.00167153	+/- 0.001651
c	= 0.821445	+/- 0.1213

Table 4: Fit of exponential to ionisation current

Figure 13 shows the third SEM target, which was placed furthest upstream. It can be seen that the contamination of the second target (next downstream) was minimal (see figure 15) there was little visible deposition on the first target - furthest downstream.

Target	Start mass	Final mass	Difference
1	= 0.2500	0.2500	0.0000
2	= 0.247(0/1)	0.247(0/1)	0.0003
3	= 0.2475	0.2478	0.0000
Filter	= 36.2402	36.2492	0.0090

Table 5: Measured mass of the SEM targets and Filter Tube before and after the flow test

It can be seen that the collection ratios are at



Figure 13: The third SEM target after the test, showing a thick coating of salt



Figure 14: The second and first targets, the second target showing a slight dusting of salt



Figure 15: The SEM targets after the second flow test, third is leftermost, first rightermost. The second showing a lighter coating of salt than the thrid, and the first only a slight dusting

least $\frac{\Delta M_3}{\Delta M_2} < \frac{1}{3}$ and possibly $< \frac{1}{6}$ from the fact that the mass of the seconds target was +/- one least significant digit both before and after the experiment. Unfortunately the limitations of the balance prevent further investigation.

Interestingly the overall efficiency is low, considerably lower than Cheng et al judging from the filter mass increase. However, some of this was shown to be due to moisture absorption by the second test results. The nebuliser was left on until ten minutes into the experieiment, and the characterisation test shows that aerosol would have continued to enter the precipitator for some time after. Using the characterisation test results it is possible to estimate how much aerosol passed through the instrument after the ionisation current dropped to zero. However the characterisation test had a longer runtime before the nebuliser was turned off, so has limited usefulness.

A second flow test was carried out to investigate efficiency further. The nebuliser and pump were turned off as soon as the ionisation current had dropped to zero, to avoid further aerosol entering the instrument. Interestingly, the filter mass was found to decrease (table 6. Leaving the filter tube in the laboratory to reach equilibrium humidity resulted in the mass increasing, confirming the hypothesis (table 7). It would appear that the filter mass absorbed 0.0006 grams of salt, however we do not know how much aerosol is removed from the airstream by impection with parts of the instrument- there was observed salt deposition on parts of the tubing. The filter mass measurement can thus only be used to put an

upper limit on the total collection efficiency of $\frac{0.0004}{0.0004+0.0006} = 40\%$.

Target	Start mass	Final mass	Difference
1	= 0.249(8/9)	0.2500	0.0000
2	= 0.246(8/9)	0.2479	0.000(0/1)
3	= 0.2474	0.2478	0.0004
Filter	= 36.2484	36.2480	-0.0004

Table 6: Measured mass of the SEM targets and Filter Tube before and after the second flow test

Time after experiment	Mass
15	36.2487
25	36.2489
54	36.2489
93	36.2490

Table 7: Filter mass in grams versus time in minutes after the filter was removed and allowed to reach humidity equilibrium with the lab air

An improved method for evaluating deposited aerosol quantities might be to dissolve in distilled water, then measure the conductivity to infer the NaCl content. Unfortunately all conductivity meters researches had insufficient accuracy to detect NaCl in the sub milligram range. Yet another technique would be to use a titration technique to find the mass of salt.

The aerosol spectrometer however offers a more powerful technique: the spectrometer was placed on the electrostatic precipitator exhaust (with the pump and filters bypassed), and the aerosol spectrum analysed with the high voltage on or off. A dilution unit being employed to reduce the particle number density to levels usable by the spectrometer.

2.6.2 Software validation

As the main flight control software was written in python to run on a linux system, it was a trivial matter to run on a ubuntu installation. In place of the pyserial module, files were used to simulate input and output from the embedded board. The most important function of the flight software is of course to enable a recovery of the payload after the flight, so GPS input needs

to be replicated, and output to the radio and phone logged for analysis. The standard protocol for GPS chipsets is NMEA, a datapacket over serial protocol, where each packet has a header, data fields of comma separated variables, and finally parity data to identify errors. The university of Wyoming have produced an online application for simulating balloon flights⁶, which produces an output in Kml, and Xml format. A simple C program posted on the UKHAS wiki⁷ was used to convert simulated flights into NMEA format. The flight code was thus tested under realistic flight conditions, allowing the landing spot prediction and polygon flight boundard, or “geofence” to be debugged, which would otherwise not have been possible.

3 conclusions

The sonde payload serves as a useful tool for atmospheric aerosol analysis, and is planned to be flown shortly by the Department.

The instrument allows three samples to be obtained at different vertical altitude ranges, but there is much room for improvement. Deposited particle density on the deposition surface is low, there is cross contamination between samples, and the overall number of samples could be increased to give greater vertical resolution.

References

- [1] D.F. Blake and K. Kato, 1995: Latitudinal distribution of black carbon soot. *Journal of geophysical research*, Vol 100, No. D4, 7195-7202
- [2] William C. Hinds, 1999, *Aerosol technology, properties, behaviour, and measurement of airborne particles*. Wiley.
- [3] R.F. Pusechel and Coauthors, 1992: Black carbon (soot) aerosol in the lower strato-

⁶This can be found at http://weather.uwyo.edu/polar/balloon_traj.html

⁷Posted at <http://wiki.ukhas.org.uk/code:emulator>

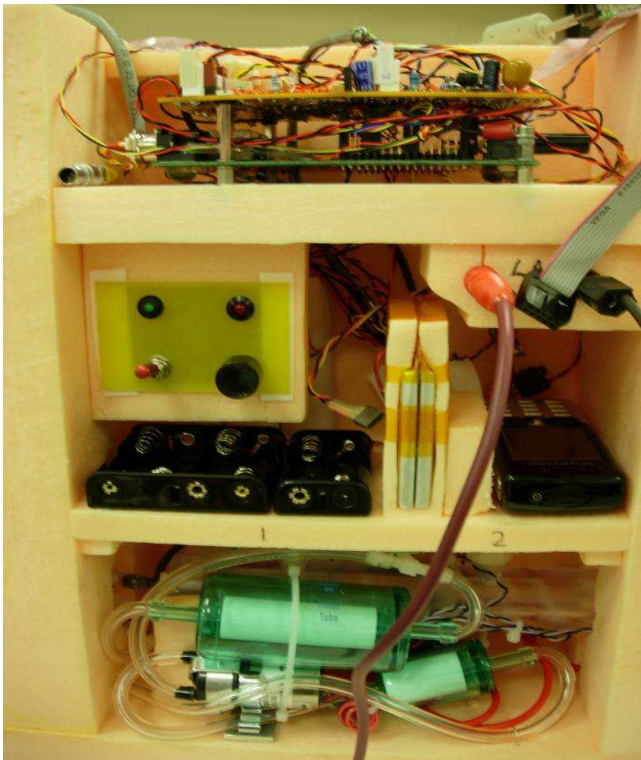


Figure 16: The assembled payload with the enclosure lid removed

sphere and upper troposphere. *Geophysical Research Lett.*, Vol 19, No. 16, 1659-1662

- [4] Brenninkmeijer, C. A. M., and Coauthors, 1999: CARIBIC- Civil aircraft for global measurement of trace gases and aerosols in the tropopause region. *J. Atmos. Oceanic Technol.*, 16, 1373-1383
- [5] Snetsinger and Coauthors, 1987: Effects of the March-April 1982 El Chichon eruption on stratospheric aerosols, late 1982 to early 1984. *Journal of Geophysical Research*, Vol 92, No. 14, 761-771
- [6] Yung-sung Cheng et al, 1981: Collection efficiencies of a point-to-plane electrostatic precipitator. *American industrial hygiene Ass. Journal*, 42, 605-610.
- [7] Alexander Laskin and James P. Cowin, 2001: On deposition efficiencies of a point-to-plane electrostatic precipitator. *Journal of aerosol science*, 33, 405-409

- [8] Morrow, P.E., & Mercer, T. T. 1964: A point-to-plane electrostatic precipitator for particle size sampling, *American industrial hygiene Ass. Journal*, 25, 8-14
- [9] <http://www.mil.ufl.edu/~chrisarnold/components/microcontrollerBoard/AVR/avrlib/>
- [10] The UK high altitude society is a not for profit umbrella organisation to facilitate co-operation between UK high altitude balloon groups- <http://www.ukhas.org.uk>
- [11] Cambridge University Spaceflight is a student organisation focused on high altitude and space flight- www.srcf.ucam.org/cuspaceflight/
- [12] <http://data.energizer.com/PDFs/l91.pdf>